

Kinetic analysis of thermal stability of human low density lipoproteins: a model for LDL fusion in atherogenesis^S

Mengxiao Lu,¹ Donald L. Gantz, Haya Herscovitz, and Olga Gursky¹

Department of Physiology and Biophysics, Boston University School of Medicine, Boston, MA 02118

Abstract Fusion of modified LDL in the arterial wall promotes atherogenesis. Earlier we showed that thermal denaturation mimics LDL remodeling and fusion, and revealed kinetic origin of LDL stability. Here we report the first quantitative analysis of LDL thermal stability. Turbidity data show sigmoidal kinetics of LDL heat denaturation, which is unique among lipoproteins, suggesting that fusion is preceded by other structural changes. High activation energy of denaturation, $E_a = 100 \pm 8$ kcal/mol, indicates disruption of extensive packing interactions in LDL. Size-exclusion chromatography, nondenaturing gel electrophoresis, and negative-stain electron microscopy suggest that LDL dimerization is an early step in thermally induced fusion. Monoclonal antibody binding suggests possible involvement of apoB N-terminal domain in early stages of LDL fusion. LDL fusion accelerates at pH < 7, which may contribute to LDL retention in acidic atherosclerotic lesions. Fusion also accelerates upon increasing LDL concentration in near-physiologic range, which likely contributes to atherogenesis. Thermal stability of LDL decreases with increasing particle size, indicating that the pro-atherogenic properties of small dense LDL do not result from their enhanced fusion. Our work provides the first kinetic approach to measuring LDL stability and suggests that lipid-lowering therapies that reduce LDL concentration but increase the particle size may have opposite effects on LDL fusion.—Lu, M., D. L. Gantz, H. Herscovitz, and O. Gursky. Kinetic analysis of thermal stability of human low density lipoproteins: a model for LDL fusion in atherogenesis. *J. Lipid Res.* 2012. 53: 2175–2185.

Supplementary key words LDL aggregation, fusion, and rupture • sigmoidal denaturation kinetics • LDL subclasses • acidic pH • high-order reaction • lipid-lowering therapies • atherosclerosis

Low density lipoproteins (LDL, also known as “bad cholesterol”) are noncovalent assemblies containing hundreds of lipids and a single copy of apolipoprotein B (apoB), a 550 kDa glycoprotein that comprises over 95% of total LDL protein (1). Plasma LDL are the major vehicles for cholesterol delivery to peripheral cells (2). Plasma levels

of LDL cholesterol and, particularly, apoB are the strongest predictors of atherosclerosis and its causative agents (3). In atherosclerosis, LDL lipids are deposited in the arterial intima; according to the response-to-retention paradigm (4, 5), LDL retention by the arterial matrix proteoglycans triggers a cascade of pro-atherogenic events culminating in formation of atherosclerotic plaque (6–8). These events include biochemical modifications of LDL, such as oxidation and/or hydrolysis by the resident proteases and lipases, e.g., phospholipase A₂ and sphingomyelinase, which can reduce LDL affinity for the LDL receptor, increase LDL affinity for the proteoglycans, and promote LDL fusion (7–14). In addition, ionic interactions with proteoglycans reduce LDL stability and promote their fusion and rupture (i.e., release of core lipids) (15). Fusion of lipoproteins prevents their exit from the arterial intima and thereby augments their further modifications, enhances LDL uptake by the arterial macrophages, and initiates the formation of atherosclerotic lesions (9, 16). Therefore, the pro-atherogenic potential of LDL is thought to be linked to their ability to fuse (9, 10, 17). Dissecting the pathogenic pathway of LDL fusion and identifying key factors that promote or inhibit this pathway can help obtain new therapeutic targets for atherosclerosis.

Structural analysis of intact and modified LDL has been limited to low resolution (≥ 16 Å) by the large size and hydrophobicity of apoB and by LDL heterogeneity (1, 18–21). Human plasma LDL consist of subclasses differing

Abbreviations: CD, circular dichroism; EM, electron microscopy; mAb, monoclonal antibody; NDGE, non-denaturing gel electrophoresis; sdLDL, small dense LDL; SEC, size-exclusion chromatography; T-jump, temperature jump.

¹To whom correspondence should be addressed.

e-mail: gursky@bu.edu (O.G.); mxlu@bu.edu (M.L.)

²In this work, “denaturation” is used to describe LDL aggregation and fusion (illustrated in supplementary Fig. 1) followed by rupture that involves release of apolar core lipids and their coalescence into droplets and phase separation. For brevity, we sometimes use “fusion” to describe these transitions. In literature, the term “aggregation” is often used to describe increase in lipoprotein size that may result from particle aggregation, fusion, and/or rupture. To differentiate among these transitions, we use electron microscopy to visualize particle size and morphology, together with near-UV circular dichroism to monitor rupture as previously described (30, 36).

^SThe online version of this article (available at <http://www.jlr.org>) contains supplementary data in the form of four figures and one table.

This work was supported by National Institutes of Health Grants GM-067260 and HL-026335. Its contents are solely the responsibility of the authors and do not necessarily represent the official views of the National Institutes of Health.

Manuscript received 19 June 2012 and in revised form 19 July 2012.

Published, JLR Papers in Press, July 31, 2012

DOI 10.1194/jlr.M029629

Copyright © 2012 by the American Society for Biochemistry and Molecular Biology, Inc.

This article is available online at <http://www.jlr.org>

in particle diameter (20–24 nm), charge, biochemical composition, apoB conformation, and metabolic properties (17, 22–24). Among these subclasses, small dense LDL (sdLDL) are thought to be particularly pro-atherogenic due to their reduced affinity to LDL receptor, increased affinity to arterial proteoglycans, and increased susceptibility to pro-atherogenic modifications, such as oxidation (23–25). Furthermore, electronegative LDL show enhanced pro-atherogenic properties (17, 26–28) that have been linked to their increased propensity to aggregate and fuse (17). The relative fusion propensity of sdLDL versus their larger counterparts remains unknown and is addressed in this work.

Although the detailed structural basis for LDL fusion is unclear, it is thought to result from accumulation of packing defects on LDL surface that form upon mechanical, thermal, chemical or enzymatic perturbations (9–15, 29–32). The latter include lipolysis of polar lipids, such as phosphatidylcholine or sphingomyelin, and proteolysis of apoB followed by dissociation of its proteolytic fragments (7–15, 32). We showed that thermal denaturation² mimics *in vivo* LDL aggregation, fusion, and rupture (i.e., release of neutral lipids from LDL core, which coalesces into droplets) (30) (supplementary Fig. 1). Thermal denaturation studies revealed that stability of LDL and other lipoproteins is determined by kinetic barriers and suggested that similar barriers modulate lipoprotein remodeling and fusion *in vivo* (30, 33–36). In fact, the products of the heat-induced LDL fusion are similar in size and morphology to LDL-derived extracellular deposits in early atherosclerotic lesions (37). To quantify LDL stability, we used a kinetic approach applied in the previous thermal stability studies of high- and very low-density lipoproteins, HDL and VLDL (34–36), and HDL subclasses (38). The application of this approach to LDL has been complicated by the relatively narrow range of experimental conditions allowing kinetic data collection. These conditions have been identified in the current work, allowing us to characterize the early stages in LDL aggregation and fusion and perform the first quantitative kinetic analysis of LDL stability. We also determined how the rate of LDL heat denaturation *in vitro* is affected by factors that can critically influence LDL fusion *in vivo*, such as LDL concentration, particle size, and pH.

MATERIALS AND METHODS

Lipoprotein and apolipoprotein preparation

Plasma of healthy volunteer donors was obtained with their written informed consent upon approval by the Institutional Review Board. Single-donor LDL were isolated from fresh plasma by KBr density gradient ultracentrifugation in the density range 1.019–1.063 g/ml following established protocols (39). LDL were dialyzed against standard buffer (20 mM Na phosphate, pH 7.5) containing 0.25 mM Na EDTA and stored in the dark at 4°C. LDL stock solution was used within four weeks during which no protein degradation was detected by sodium dodecyl sulfide polyacrylamide gel electrophoresis (SDS-PAGE). LDL subclasses differing in particle density were separated from total LDL by KBr density gradient ultracentrifugation in the following density ranges:

1.025–1.034 g/ml for LDL₁ (large buoyant), 1.034–1.044 g/ml for LDL₂ (mid-range), and 1.044–1.060 g/ml for LDL₃ (small dense) (24). The separation was confirmed by negative-stain electron microscopy (EM). Unless otherwise stated, total LDL and their subclasses in standard buffer were used for further studies. The protein concentration in LDL was measured by using a modified colorimetric Lowry assay (40).

Particle size analysis during thermal denaturation

Size-exclusion chromatography (SEC) was used to assess particle size distribution at various stages of thermal denaturation and to isolate lipoprotein fractions differing in the particle size. LDL samples (0.5 mg/ml protein in standard buffer) that have been subjected to various thermal treatments were filtered using 0.2 µm filter and applied to Superose 6 10/300 GL column (GE Healthcare). The samples (100–500 µl injection volumes) were eluted with a standard buffer at a flow rate of 0.5 ml/min. Elution of lipoproteins was monitored by absorbance at 280 nm. Fractions were collected and analyzed by nondenaturing PAGE (NDGE) and EM to determine particle size.

For negative-stain EM, LDL subjected to various thermal treatments were stained using 1% w/v sodium phosphotungstate at pH 7.5, 22°C, and were visualized under low-dose conditions by using a CM12 transmission electron microscope (Philips Electron Optics) as described (34). Digital images were collected at 56,250 magnification with a Teitz 1K × 1K CCD camera (Gauting, Germany). Particle size analysis was carried out by using PHOTO-SHOP computer graphics with EXCEL program using ~300 particles per image.

Gel electrophoresis and immunoblotting

Total LDL at various stages of thermal denaturation and their fractions isolated by SEC were analyzed by 4% NDGE and SDS-PAGE to assess particle size and apoB aggregation and/or proteolysis, respectively, and by Western blotting to detect possible changes in epitope exposure upon LDL aggregation. Native and nonnative gels were run at 150 V for 1.5–2 h, followed by Coomassie blue staining. ApoB was detected by immunoblotting following NDGE. Proteins were transferred to polyvinylidene fluoride membrane for 1.5 h at 100 V or for 24 h at 30 V, incubated in blocking buffer (non-fat milk buffer containing 10 mM Tris HCl, pH 7.5, 0.1% v/v 150 mM NaCl, 0.05% w/v Tween-20), and probed with primary monoclonal antibodies (mAbs) to apoB100 followed by horseradish peroxidase-conjugated secondary antibodies. The blots were visualized using an enhanced chemiluminescent system (Perkin Elmer). We used nine mAbs to apoB100 N- and C-terminal domains that are expected to undergo structural changes during LDL fusion. These mAbs and their epitopes, which are shown in supplementary Fig. III and supplementary Table I, include Mb19 (71), Mb24 (405–539), 1D1 (474–539), Mb11 (1022–1031), Mb47 (3429–3453 and 3507–3523), 5E11 (3441–3569), 4F6 (3569–3925), Mb43 (4027–4081), and B_{sol}7 (4517–4536). All mAbs were a kind gift by Dr. David Atkinson from Boston University School of Medicine, except for 1D1 that was purchased from the University of Ottawa Heart Institute.

Circular dichroism and turbidity measurements

AVIV-400 and AVIV-62DS spectropolarimeters were used to record circular dichroism (CD) and turbidity data. Unless otherwise stated, the lipoprotein samples containing 0.5 mg/ml protein in standard buffer were placed in 5 mm path length cells. To characterize secondary structure of apoB at various stages of thermal denaturation, far-UV CD spectra were recorded at 190–250 nm with 1 nm bandwidth, 1 nm increment, and 30 s/nm accumulation time. Far-UV CD data were normalized to protein concentration

and expressed as molar residue ellipticity, $[\Theta]$, in units of $\text{degrees}\cdot\text{cm}^2\cdot\text{dmol}^{-1}$.

Thermal stability of LDL was assessed in the melting or kinetic experiments. Turbidity, which was recorded by using dynode voltage, V , in CD experiments as described (33), was used to monitor increase in the particle size upon LDL aggregation, fusion, and rupture. Near-UV CD was used to monitor LDL rupture and release of apolar lipids that coalesce into lipid droplets, which induced a large negative CD peak centered near 320 nm (30, 36). Near-UV CD and turbidity were measured simultaneously at 320 nm. In kinetic temperature-jump (T-jump) experiments, LDL heat denaturation was triggered at time $t = 0$ by a rapid increase in temperature from 4°C to a higher constant value. T-jump data recorded using different initial temperatures (4°C, 25°C, or 37°C), but the same final temperature closely overlapped. The time course of denaturation was monitored with 10 s increments for up to 21 h. In the melting experiments, the samples were heated and cooled at a rate of 11°C/h with 1°C increment. No changes in the sample volume, protein concentration, or protein or lipid oxidation status were detected after heating and cooling (30).

Kinetic analysis of LDL thermal stability

ORIGIN software was used for the data analysis and graphic representation. The turbidity data, $V(t)$, recorded in T-jumps to each temperature were approximated by a sigmoidal function:

$$V(t) = V_0 + (V_1 - V_0) / \left\{ 1 + \exp\left[\frac{t - t_{1/2}}{k}\right] \right\}$$

Here, V_0 is the initial turbidity of intact LDL, V_1 is the asymptotic value corresponding to denatured LDL, $t_{1/2}$ is the reaction midpoint corresponding to 50% change in turbidity, and k is the rate constant. The results were analyzed by using an Arrhenius model as described previously (33). The Arrhenius plots, $k(T)$ versus $1/T$, where T is temperature in Kelvin, were approximated by linear functions whose slopes were used to determine the Arrhenius activation energy (enthalpy), E_a , of LDL denaturation. The value of E_a reflects the number and character of packing interactions per cooperative unit that are transiently disrupted during lipoprotein heat denaturation. Cooperative unit in model HDL probably contains one protein molecule and adjacent lipids (Ref. 41 and references therein). Cooperative unit in LDL heat denaturation remains to be determined; we speculate that it involves a portion of apoB and adjacent lipids.

All experiments in this study were repeated at least three times to ensure reproducibility.

RESULTS

Quantitative kinetic analysis of LDL thermal stability

Thermal stability of LDL was determined by using an Arrhenius analysis of the heat denaturation. To establish experimental conditions allowing kinetic data collection in a temperature range broad enough for an accurate Arrhenius analysis, we explored a range of LDL concentrations (0.1–1.5 mg/ml protein), salt concentrations (0–150 mM NaCl or Na phosphate), pH (6.0–8.0), and temperatures (20°C–98°C). Under most conditions, the time scale of LDL fusion was either too fast (<2 min) or too slow (>10 h) to be accurately measured by using steady-state CD spectroscopy. Good kinetic data were obtained using LDL

solutions of 0.5 mg/ml protein concentration in 20 mM Na phosphate buffer, pH 7.5. These standard conditions were used to record the data shown in Figs. 1–5.

Figure 1 shows the first kinetic analysis of LDL stability. Thermal denaturation of freshly isolated LDL was triggered in T-jumps from 4°C to higher constant temperatures, 75°C to 85°C (Fig. 1A), and was monitored by turbidity (dynode voltage, V) as described (33, 36). LDL heat denaturation showed sigmoidal time course that contrasts with the exponential decay time course observed in other lipoproteins (33–36). At each temperature, the turbidity data, $V(t)$, in Fig. 1A were approximated by a sigmoidal function to determine the reaction midpoint $t_{1/2}$ and the rate constant k as described in Materials and Methods and illustrated in Fig. 2A. The results were used to obtain Arrhenius plot, $\ln k(T)$ versus $1/T$, as well as the plot of $\ln t_{1/2}(T)$ versus $1/T$ (Fig. 1B). The slopes of these plots were similar within the error of their experimental determination, indicating similar temperature dependence of the lag phase (that contributes to $t_{1/2}$) and the transition phase of LDL denaturation (that influences both k and $t_{1/2}$). The activation energy determined from the slope of the Arrhenius plot was $E_a = 100 \pm 8$ kcal/mol. The uncertainty in this value incorporates the fitting errors and the deviations among the data sets recorded from different batches of LDL. Notably, this value of E_a is nearly twice as high as the maximal values obtained from heat denaturation studies of human HDL (35) or VLDL (36). High activation energy of LDL denaturation reflects a steep temperature dependence of its rate constant, $k(T)$, and explains why LDL heat denaturation could be monitored in a relatively narrow temperature range. In summary, the results in Fig. 1 revealed sigmoidal kinetics and high activation energy of LDL denaturation that have not been observed in any other lipoproteins.

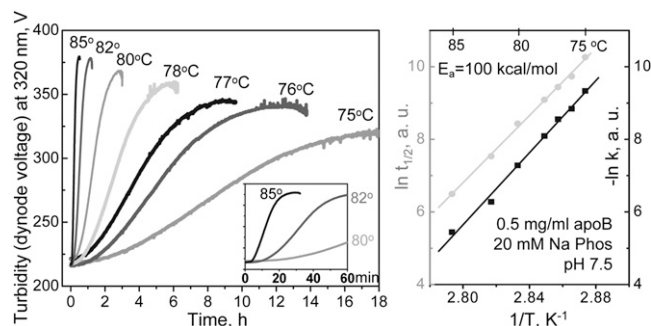


Fig. 1. Kinetic analysis of thermal stability of human LDL. (A) Freshly isolated single-donor LDL under standard conditions (0.5 mg/ml protein in 20 mM Na phosphate, pH 7.5) were subjected to temperature jumps (T-jumps) from 4°C to higher temperatures ranging from 75 to 85°C as indicated. The time course of LDL thermal denaturation was monitored by turbidity at 320 nm. Insert shows zoomed-in portions of the data recorded during the first 60 min of LDL incubation at 80°C, 82°C, or 85°C. Each data set was approximated by a sigmoidal function to determine the rate constant k and the transition midpoint $t_{1/2}$. (B) Arrhenius analysis of the turbidity data. The plots $\ln k(T)$ versus $1/T$ (black) and $\ln t_{1/2}$ versus $1/T$ (gray) have similar slopes corresponding to an Arrhenius activation energy of $E_a = 100 \pm 8$ kcal/mol.

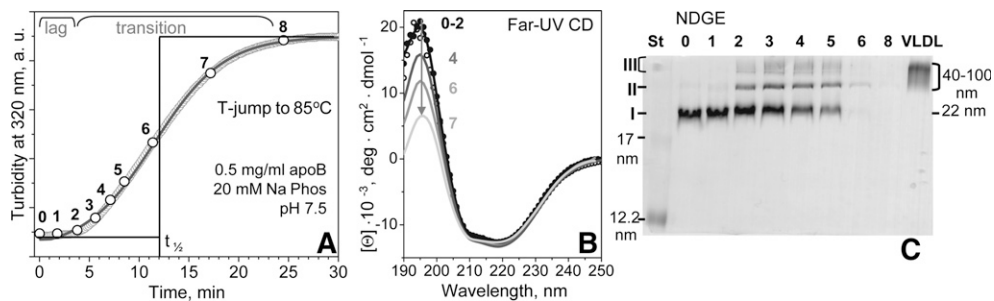


Fig. 2. Characterization of total LDL at various stages of thermal denaturation. LDL sample under standard conditions was subjected to a T-jump from 4°C to 85°C, and LDL heat denaturation was monitored by turbidity (A). Aliquots of 40 μ l taken at various time points are numbered from 0 (intact LDL) to 8 (fully denatured LDL). Each aliquot was diluted to 0.1 mg/ml protein and placed in a 1 mm path length cell to record a far-UV CD spectrum (B). The CD spectra of aliquots 0 (black dots), 1 (black line), and 2 (gray dots) fully overlapped. The major spectral changes observed at later stages of heat denaturation (numbered) are shown by the arrow. NDGE of LDL at various stages of heat denaturation (C). Lane numbers 0–8 correspond to aliquot numbers in panel A. St, molecular size standard; data for intact human VLDL (particle diameter 40–100 nm) are shown for comparison. Three major bands observed in the heat-denatured LDL are marked I–III.

Structural changes during thermal denaturation of LDL

To identify structural changes at specific stages of LDL heat denaturation, an LDL sample under standard conditions was subjected to a T-jump to 85°C. Aliquots were taken at various times (shown by numbers in Fig. 2A) and were analyzed by far-UV CD (Fig. 2B), NDGE (Fig. 2C), and negative-stain EM (Fig. 3) to determine secondary structure, particle size, and particle morphology, respectively. During the lag phase (i.e., prior to significant changes in turbidity), no changes in far-UV CD were observed, indicating that there were no large secondary structural changes in apoB (0–2) (Fig. 2A, B). In the transition phase corresponding to an increase in turbidity and, hence, increased particle size, far-UV CD spectra showed a progressive reduction in intensity below 208 nm (4–7) (Fig. 2B). This could potentially result from two effects: *i*) increased light scattering upon increasing the particles size, which disproportionately reduces CD intensity at short wavelengths and thereby distorts far-UV CD spectra of large particles (42); and/or *ii*) partial unfolding of the secondary structure in apoB upon heating (30, 36). Notably, the CD spectra in Fig. 2B showed little changes at 208–250 nm, indicating that, consistent with our earlier studies (30),

apoB retained most of its secondary structure after prolonged incubation of LDL at high temperatures.

NDGE revealed incremental changes in the particle size during incubation at 85°C (Fig. 2C). At stage 1, the particle size distribution appeared unchanged (lanes 0 and 1), with the sole band I similar to that observed in intact LDL (average diameter $\langle d \rangle = 22$ nm). At stages 2–5, two additional bands were observed: a sharp band II corresponding to hydrodynamic size circa 40 nm, and a diffuse band III encompassing a broad range of sizes larger than 80 nm (lanes 2–5). At stages 6 and beyond [i.e., near the transition midpoint $t_{1/2}$ measured by turbidity (Fig. 1A)], few if any lipoproteins entered the gel (Fig. 2C, lanes 6–8). This is consistent with earlier EM observation of LDL aggregation, fusion, rupture, and release of apolar core lipids that coalesce into lipid droplets at advanced stages of denaturation (30) (illustrated in supplementary Fig. 1). Notably, SDS-PAGE showed that heat denaturation of LDL does not cause apoB fragmentation but induces gradual formation of apoB aggregates during the transition phase (data not shown), in good agreement with NDGE and EM results.

Figure 3 shows negative-stain EM of total LDL at various stages of thermal denaturation. Electron micrographs of

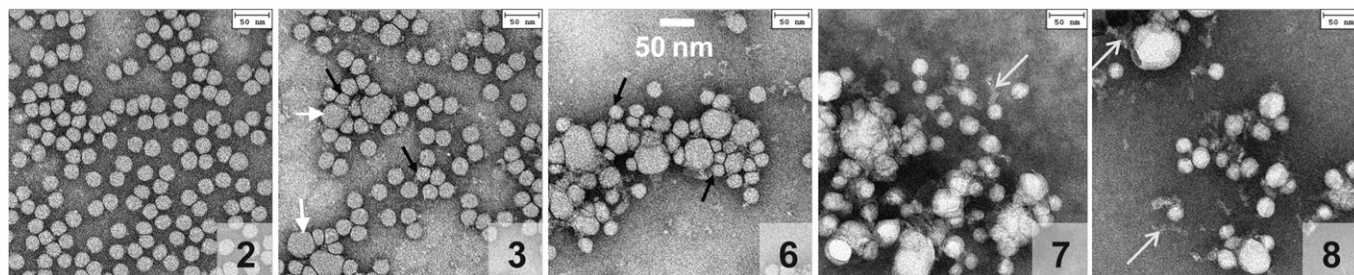


Fig. 3. Electron micrographs of negatively stained total plasma LDL at various stages of thermal denaturation. Aliquots were taken at different times of incubation at 85°C as described in Fig. 2. Panel numbers correspond to the denaturation stages in Fig. 2. Each aliquot was cooled to 22°C, diluted to 50 μ g/ml protein, and visualized by negative-staining EM. Intact LDL (not shown) and LDL that had been incubated at 85°C for 4 min (2) or less were indistinguishable by EM; other micrographs show LDL that have been incubated at 85°C for 6 min (3), 12 min (6), 17 min (7), or 24 min (8). Short white arrows point to fused LDL, black arrows to particles that are smaller than intact LDL, and long white arrows to electrolucent strands whose morphology is consistent with dissociated apoB.

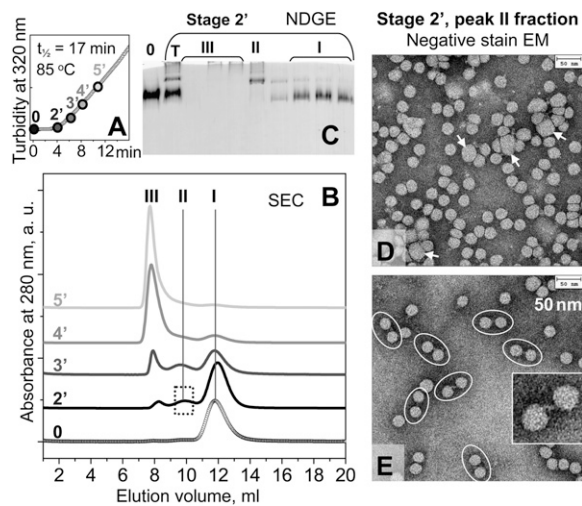


Fig. 4. Morphological analysis of LDL at early stages of heat denaturation. (A) LDL sample under standard conditions was subjected to a T-jump from 4°C to 85°C, and LDL fusion was monitored by turbidity at 320 nm. Aliquots were taken at different incubation times at 85°C, from 2' (200 sec) to 5' (500 sec) prior to the denaturation midpoint ($t_{1/2}$ = 17 min for this sample); 0 stands for intact LDL. (B) SEC of selected aliquots (0, 2', 3', 4', 5') that were eluted with 20 mM Na phosphate, pH 7.5. Three major peaks in the SEC profile are marked I, II, and III. The results agree with the earlier SEC studies of LDL showing increased particle size upon heat denaturation (43). (C) NDGE of LDL sample at denaturation stage 2'. SEC fractions encompassing peaks I, II, and III are numbered. T, total plasma LDL; 0, intact LDL. (D, E) Negative-stain electron micrographs of peak II isolated by SEC from LDL at stage 2'. The sample was diluted to protein concentration of 100 µg/ml (D) or 20 µg/ml (E) prior to deposition on the grid. Arrows show enlarged (fused) particles, and ovals show intact-sized LDL tethered in pairs. Insert shows a zoomed-in pair of LDL particles and their connecting strand (E).

total LDL that were intact (0) or were taken at stages 1 or 2 of the lag phase (Fig. 3, panel 2) were indistinguishable. At stage 3 corresponding to the beginning of the transition phase, the particles became heterogeneous in size, with a significant population of enlarged lipoprotein-like particles ($d \sim 40$ nm) that were apparent products of LDL fusion (Fig. 3, panel 3, white arrows). This trend continued upon progression of denaturation when smaller (black arrows) and larger particles with progressively increasing radii as well as their aggregates were observed (panels 6–8). In addition, thin electrofluorescent strands whose size and morphology were consistent with dissociated apoB were detected at advanced stages of heat denaturation in this (panels 7 and 8, long white arrows) and earlier LDL studies (30). In summary, NDGE and negative-stain EM of total LDL agreed with the turbidity data (Figs. 2 and 3) and showed changes in the particle size upon thermal denaturation. These changes include formation of smaller and larger particles and their aggregates, in good agreement with our earlier studies of LDL (30). A novel result was a sharp band observed by NDGE at denaturation stages 2–5, which corresponded to the particle size circa 40 nm (Fig. 2C, band II). A similar sharp band was detected by NDGE in LDL subjected to other perturbations, such as chemical denaturation or hydrolysis upon prolonged storage at 4°C

(supplementary Fig. IV). This suggests that band II represents a universal early stage in LDL denaturation by various physical or chemical perturbations. The position of band II on NDGE suggests that it is probably composed of a small number of aggregated and/or fused LDL whose identity is beginning to be addressed in the next section.

Structural studies of LDL at early stages of aggregation and fusion

SEC was used to isolate and characterize LDL at early stages of thermal denaturation. LDL under standard conditions were subjected to a T-jump to 85°C, and aliquots were taken during the first 11 min of incubation (stages 2'–5') (Fig. 4A), i.e., before the transition reached its midpoint measured by turbidity, $t_{1/2}$ = 17 min. As expected, SEC profile of intact LDL showed a single peak with elution volume circa 12 ml (peak I) corresponding to NDGE band I (Fig. 4C, lane 0). SEC profile of LDL denatured to stage 2' (end of the lag phase) showed two additional peaks: peak II centered near 9.5 ml and peak III near 8 ml corresponding to the void volume (Fig. 4B, line 2'). At stage 3' (early transition phase), peak III increased in intensity, peak II showed little change, and peak I decreased (Fig. 4B, line 3'). This increase in peak III at the expense of peak I continued until peak III became the sole feature in the SEC profile at relatively advanced stages of LDL heat denaturation (stage 5' and beyond).

Next, LDL were denatured to stage 2', and peak fractions I, II, and III were isolated by SEC and analyzed by NDGE (Fig. 4C). The results were consistent with NDGE of total LDL (Fig. 2C) and clearly showed that *i*) SEC peak I and NDGE band I encompassed intact-sized LDL ($d \sim 22$ nm); *ii*) SEC peak II corresponded to the sharp NDGE band II (hydrodynamic size ~ 40 nm); and *iii*) SEC peak III corresponded to the broad NDGE band III encompassing particle sizes from about 80 nm to over 100 nm.

Negative-stain EM of peak fractions I–III isolated by SEC from LDL denatured to stage 2' confirmed this conclusion and showed that peak I contained intact-sized LDL, while peak III contained clusters of aggregated and fused particles and lipid droplets (supplementary Fig. II) similar to those observed by EM of total LDL at advanced stages of thermal denaturation (Fig. 3, panels 6–8). Notably, EM of peak II fraction showed mainly intact-sized LDL (Fig. 4D, E) even though NDGE detected only larger-sized particles (Fig. 4C, lane II), suggesting that peak II contained low-order LDL aggregates. This idea was supported by EM analysis of peak II fraction taken at various dilutions (Fig. 4D, E). At a relatively high sample concentration (100 µg/ml protein), EM of peak II fraction showed mainly clusters of intact-sized LDL, along with a small population of fused particles with diameters $d \sim 40$ nm (Fig. 4D, white arrows). To minimize lipoprotein clustering, the sample was diluted to 20 µg/ml protein prior to deposition on the EM grid. The EM results showed mainly intact-sized LDL, most of which appeared in pairs tethered via the connecting strands (Fig. 4E, ovals). Occasional fused particles, such as those seen in Fig. 4D (white arrows), were detected. Notably, electron micrographs of intact LDL under similar conditions showed

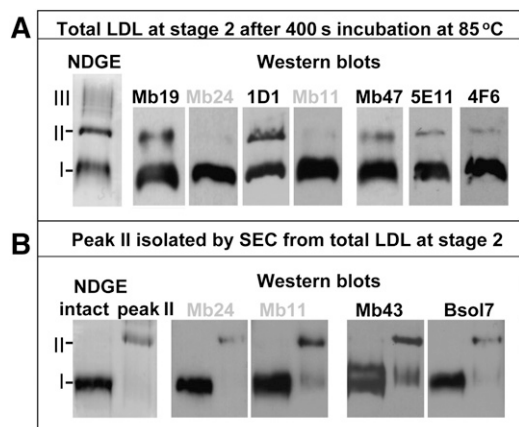


Fig. 5. Immunochemical analysis of LDL at an early stage of thermal denaturation. (A) LDL solution under standard conditions was incubated for 400 sec at 85°C as described in Fig. 4 and analyzed by NDGE followed by immunoblotting using mAbs that bind to epitopes from the N- or the C-terminal thirds of apoB. Three major bands corresponding to SEC peaks I, II, and III in Fig. 4 are indicated on NDGE (left). Western blots show mAbs binding to bands I and II. (B) Peak II fraction isolated by SEC was subjected to NDGE and immunoblotting using selected mAbs. The results for peak I are shown for comparison. The epitopes for mAbs used in this work are shown in supplementary Table I and supplementary Fig. III.

mainly single particles (data not shown), suggesting that LDL pairing at stage 2' resulted, at least in part, from thermal modifications rather than from the artifacts of the negative stain. Taken together, NDGE, SEC, and EM data in Figs. 3 and 4 suggest that peak II is probably comprised of fused or aggregated LDL particles.

In an attempt to identify apoB regions involved in LDL aggregation and fusion, we tested whether binding of mAbs to specific epitopes of apoB was affected by the heat-induced changes in LDL morphology at early stages of thermal denaturation. The mAbs used in this work targeted the apoB epitopes from the N- and C-terminal domains (supplementary Figure III and supplementary Table I); these domains are located in proximity on LDL surface and are expected to undergo structural changes upon LDL aggregation and/or changes in the particle size (Refs. 18–21, 28 and references therein). First, LDL were subjected to a T-jump to 85°C, and an aliquot taken at the end of lag phase (Fig. 4A, stage 2') was analyzed by NDGE and immunoblotting. Representative results are shown in Fig. 5A. Most mAbs clearly showed binding to the LDL species comprising bands I and II, except for MB24 and MB11 that showed minimal binding to band II. To further explore the binding of these and other antibodies to the dimeric/fused LDL comprising band II, peak II fraction was isolated by SEC and analyzed by immunoblotting. Representative results are shown in Fig. 5B. These and other results show that all mAbs explored bound to the early intermediate of LDL aggregation/fusion (band II). Therefore, quantitative affinity studies using a wide array of antibodies will be needed to identify apoB epitopes that undergo structural changes prior or during LDL aggregation and fusion. These future studies, together with the

analyses of other LDL proteins and lipids, will determine whether band II is formed by a subset of LDL with distinct biochemical and structural properties or whether it is a universal early intermediate of LDL denaturation.

Effects of LDL concentration, particle size, and pH on the rate of LDL heat denaturation

In the next series of experiments, we applied the kinetic approach developed in Fig. 1A to test how selected factors that are expected to contribute to LDL fusion *in vivo* affect the rate of LDL denaturation *in vitro*. **Figures 6–8** show the results of such experiments addressing the role of LDL concentration, particle size, and pH.

Because LDL denaturation involves aggregation, fusion, and coalescence of many particles, it is expected to be a high-order reaction. To assess the reaction order, we determined the effect of LDL concentration on the denaturation kinetics in the range encompassing 0.5 mg/ml apoB approximately corresponding to 1 mg/ml LDL cholesterol, which is considered borderline between normal and elevated plasma levels and is often used as a target value for the lipid-lowering therapies (25, 43). Earlier studies of LDL heat denaturation monitored by turbidity during heating at a constant rate showed that increasing LDL concentration from 1.5 to 4.0 mg/ml protein reduced the apparent transition temperature by nearly 20°C and thereby greatly enhanced LDL fusion (30). Kinetic analysis of the current work supported this observation and showed that increasing LDL concentration greatly accelerates fusion. This is illustrated in Fig. 6A showing the denaturation time course monitored by turbidity in a T-jump to 85°C under standard buffer conditions and LDL protein concentrations ranging from 0.15 to 1.0 mg/ml. The results reveal that increasing LDL concentration from 0.15 to 1.0 mg/ml protein leads to an approximately 20-fold increase in the

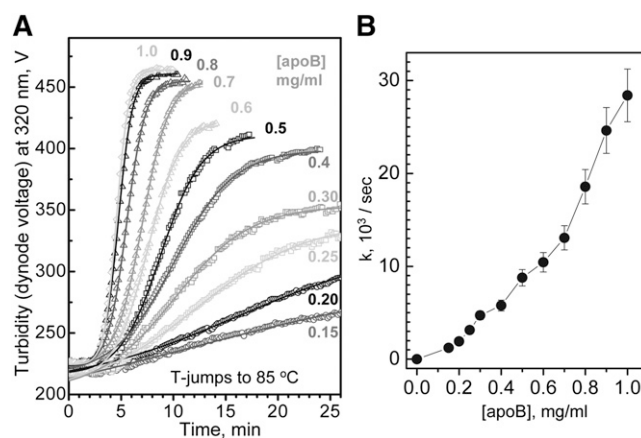


Fig. 6. Concentration dependence of LDL fusion. (A) LDL samples containing 0.15–1.0 mg/ml protein in standard buffer were subjected to T-jumps from 4°C to 85°C, and the time course of LDL denaturation was monitored by turbidity. LDL protein concentrations are indicated. Solid lines show data fitting by sigmoidal functions that were used to determine fusion rates as described in Materials and Methods. (B) Fusion rates, k , as a function of LDL protein concentration. The nonlinear plot suggests that LDL fusion is a high-order reaction.

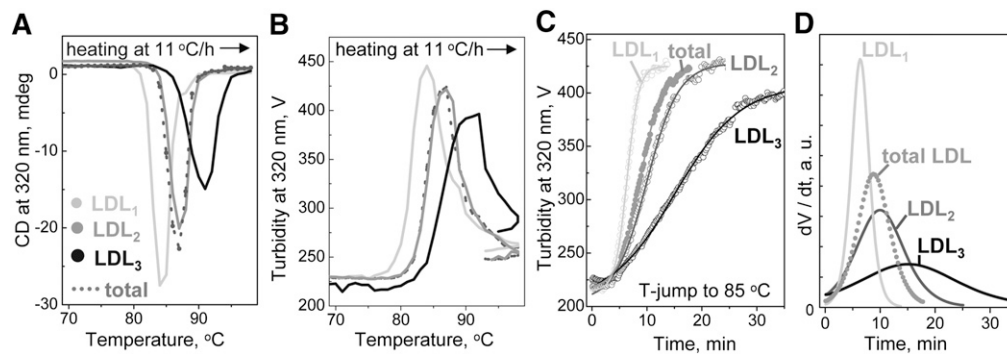


Fig. 7. Effect of the particle size on LDL stability. LDL subclasses were isolated from total LDL by density gradient centrifugation, as described in Materials and Methods, from LDL₁ (large buoyant) to LDL₃ (small dense). Relative thermal stability of these subclasses was analyzed under standard conditions in melting (A, B) or kinetic (C) experiments. LDL denaturation was monitored by near-UV CD (A) or turbidity (B, C). Near-UV CD develops a large negative signal circa 320 nm upon lipoprotein rupture and coalescence of apolar core lipids into droplets (30). A sharp decline in the amplitude of turbidity and near-UV CD following lipoprotein rupture reflects sample loss upon phase separation (30, 36). The data for total LDL are shown for comparison. The kinetic T-jump data were approximated by sigmoidal functions (solid lines in panel C); the first derivatives of these functions, $dV(t)/dt$, are shown in panel D. The results reveal that fusion of total LDL cannot be represented as a sum of transitions of individual LDL subclasses, indicating that LDL from different subclasses interact during fusion.

rate of thermal denaturation (Fig. 6B), indicating high-order reaction. Although the quality of our kinetic data was insufficient to measure the reaction order, the nonlinear plot of the denaturation rate constant k versus $[apoB]$ suggests that LDL denaturation is higher than a second-order reaction (Fig. 6B). These results imply that the rate of LDL denaturation is limited by the rate of the particle collision; hence, increasing LDL concentration increases the collision rate and thereby accelerates LDL fusion.

To test the effects of the particle size on thermal stability of LDL, intact plasma LDL were isolated by density into subclasses, from LDL₁ (large buoyant) to LDL₃ (small dense) (44); particle size was confirmed by EM (data not shown). Fig. 7 shows representative melting and kinetic data obtained from these subclasses under standard conditions. The melting data were recorded during heating at a rate of 11°C/h by turbidity and by near-UV CD (30, 36, 45). Near-UV CD was used to monitor repacking of apolar core lipids upon lipoprotein rupture and coalescence into lipid droplets, which induces a large negative CD peak centered near 320 nm (30). Fig. 7A, B show selected melting data, and Fig. 7C shows kinetic data of LDL subclasses recorded by turbidity in a T-jump to 85°C. The results reveal that, under otherwise identical conditions, larger LDL have lower apparent melting temperature (Fig. 7A, B) and denature faster than smaller LDL (Fig. 7C). Therefore, larger LDL are less stable and more prone to heat-induced fusion and rupture than their smaller counterparts.

Furthermore, the kinetic turbidity data of LDL subclasses are not additive. This is illustrated in Fig. 7D showing the first derivatives of the sigmoidal functions, $dV(t)/dt$, obtained by fitting the T-jump data, $V(t)$, recorded from total LDL and its individual subclasses. The dV/dt function of total LDL shows a single peak rather than a weighted average of individual peaks corresponding to LDL₁, LDL₂, and LDL₃ (Fig. 7D). This nonadditive behavior indicates

interactions among LDL subclasses and suggests that they can fuse with each other. Taken together with a similar nonadditive behavior of human HDL subclasses during heat denaturation (46) and with the demonstrated ability of HDL or its major protein apoA-I, to inhibit LDL aggregation and fusion (29, 47–49), this result indicates that different lipoprotein classes and subclasses interact with each other during fusion.

The effects of pH on LDL thermal stability were tested at pH 6.0–8.0 using standard concentrations of buffer and LDL (0.5 mg/ml apoB) in the melting and kinetic experiments. Figure 8 shows representative thermal denaturation data recorded by turbidity and near-UV CD. The melting data show that reduction in pH leads to a progressive decrease in the apparent transition temperature, from $\sim 100^\circ\text{C}$ at pH 8.0 to $\sim 75^\circ\text{C}$ at pH 6.0 (Fig. 8A, B), indicating LDL destabilization at acidic pH. The kinetic data further support this result and show much faster LDL fusion at lower pH (Fig. 8C). At pH 6.0, LDL were marginally stable and gradually fused at 22°C, which limited the pH range explored in our thermal stability studies. Although the lag phase was observed at any pH, the reaction time course often deviated from sigmoidal at pH 8. To compare the reaction kinetics at pH 6.0–8.0, we used the reaction midpoint $t_{1/2}$ that correlates inversely with the rate constant k (Fig. 1B). As $t_{1/2}$ corresponds to 50% change in amplitude regardless of the reaction time course, it is well suited for comparison of sigmoidal and nonsigmoidal transitions. The kinetic data in Fig. 8C suggest a nearly 40-fold reduction in $t_{1/2}$ upon reduction in pH, from ~ 90 min at pH 8.0 to 2.4 min at pH 6.0. The plot of inverse $t_{1/2}$ versus pH showed that LDL fusion greatly accelerates at mildly acidic pH (Fig. 8D). This result agrees with studies by Oorni and colleagues showing that mildly acidic pH promotes LDL fusion by sphingomyelinase at near-physiologic temperatures (Ref. 47 and references therein). Taken

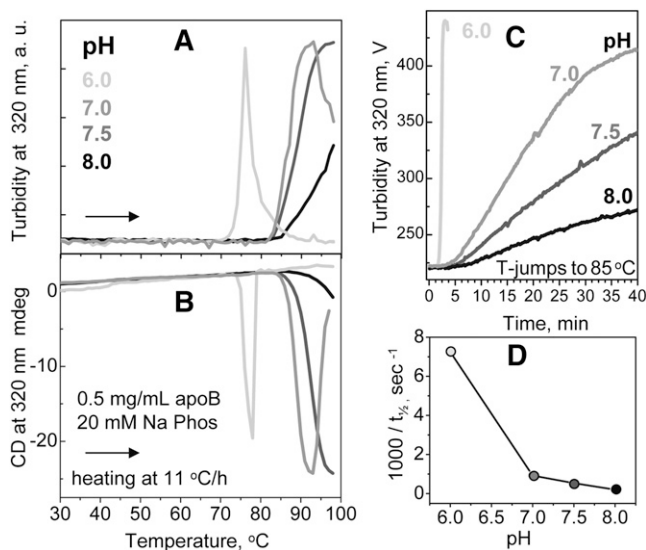


Fig. 8. Effects of pH on LDL stability. Total plasma LDL (0.5 mg/ml protein, 20 mM Na phosphate buffer, pH 6.0–8.0 as indicated) were analyzed for thermal stability in melting (A, B) or kinetic (C) experiments. In melting experiments, LDL were heated at a constant rate of 11°C/h and particle fusion and/or rupture was monitored at 320 nm by turbidity (A) and by near-UV CD (B). In kinetic experiments, LDL were subjected to a T-jump to 85°C (C). Values of inverse $t_{1/2}$ determined from these T-jump data are plotted as a function of pH (D).

together, these results show that LDL fusion upon various perturbations (thermal, enzymatic) is greatly enhanced upon reduction in pH below pH 7.

DISCUSSION

The role of LDL aggregation and fusion in atherogenesis and the effects of various LDL perturbations (thermal, mechanical, hydrolytic, acidic pH, binding by proteoglycans, etc.) are well documented in the studies by many teams, including Kovanen, Oorni, Camejo and Hurt-Camejo, and their colleagues. Here, we report the first quantitative kinetic analysis of LDL stability (Fig. 1) and show that thermal denaturation accelerates upon increasing LDL concentration (Fig. 6), increasing particle diameter (Fig. 7), and decreasing pH (Fig. 8). Thus, our work provides a tool for quantitative analysis of kinetic LDL stability under various conditions. We also report sigmoidal time course of LDL denaturation that was not observed before in any other lipoproteins.

Fusion kinetics of LDL and other lipoproteins compared

Comparison of the thermal denaturation kinetics of human LDL reported here with our earlier thermal stability studies of HDL and VLDL revealed several unique features. First, the thermal or chemical denaturation of HDL and VLDL followed hyperbolic time course without the lag phase (34–36), in contrast to the sigmoidal time course with the lag phase observed in LDL (Figs. 1A and 2A). Second, the highest activation energy observed in HDL and VLDL denaturation was circa 50–53 kcal/mol (35, 36), as

compared with $E_a = 100 \pm 8$ kcal/mol determined for LDL (Fig. 1B). Third, the rate constant of HDL denaturation measured in our studies was independent of the lipoprotein concentration in the range explored (0.15–1.0 mg/ml protein), suggesting first-order reaction, in stark contrast with LDL heat denaturation that was an apparent high-order reaction (Fig. 6). Concentration dependence of VLDL heat denaturation (36) appeared intermediate between that of HDL and LDL. We propose that these differences result, at least in part, from the distinct protein composition in LDL (that contain almost exclusively the nonexchangeable apoB), HDL (that contain only exchangeable proteins, mainly apoA-I), and VLDL (that contain comparable amounts of exchangeable and nonexchangeable proteins). Although the role of other LDL constituents cannot be excluded, we hypothesize that the unique kinetic properties of LDL aggregation, fusion, and rupture reflect mainly the large size and high hydrophobicity of apoB whose single copy comprises over 95% of total LDL protein.

Our studies of recombinant HDL showed that the activation energy of lipoprotein denaturation, which reflects transient disruption of the protein and lipid packing interactions, depends upon the apolipoprotein and lipid composition and increases from about 22 to 50 kcal/mol with increasing protein size from 6.6 to 28 kDa, apoC-I < apoA-II_{monomer} < apoA-II_{dimer} < apoA-I (41, 45). We speculate that the relatively high activation energy of LDL denaturation (Fig. 1B) probably reflects transient disruption of protein and lipid packing interactions involving relatively large parts of apoB.

Accumulative evidence suggests that LDL fusion results from major perturbations of the protein and/or lipid on the amphipathic lipoprotein surface. This may include extensive lipolysis of phospholipids, hydrolysis of apoB with release of proteolytic fragments, and chemical or thermal denaturation (9–16, 29–32, 47–49). Some of these perturbations have been proposed to involve conformational changes in apoB, particularly its N- and C-terminal domains (28, 47). The enormous size of apoB prompts us to hypothesize that its structure is kinetically trapped by both protein-lipid and protein-protein interactions. The latter is supported by several lines of evidence, including the preservation of substantial secondary structure in apoB upon thermal denaturation of LDL (Fig. 2B) (30) and preservation of immunoreactivity and the overall domain structure of apoB upon LDL delipidation by nonionic detergents (18, 50). Possible presence of multiple kinetic traps in the conformational landscape of apoB suggests that multiple incremental structural changes in this large hydrophobic protein may be needed to initiate LDL fusion. These incremental changes probably accumulate during the lag phase in our T-jump experiments. The activation energy for these structural changes is provided by the particle collisions (addressed below).

Exchangeable apolipoproteins are much smaller and less hydrophobic than apoB, and hence, they dissociate from the lipoprotein surface relatively easily; such dissociation is tightly coupled to lipoprotein fusion (33, 35, 36, 45).

This suggests that only one or a small number of lipoprotein collisions at high temperatures can cause dissociation of an exchangeable protein and lipoprotein fusion. This helps explain the absence of the lag phase observed in HDL and VLDL heat denaturation (35, 36). Furthermore, earlier studies of VLDL heat denaturation revealed two-phase kinetics, with exchangeable proteins dissociating in the faster phase, followed by partial dissociation of apoB in the slower phase (36). Taken together with the current work, these results suggest that the lag phase in VLDL denaturation is masked by the faster kinetic phase; this helps explain the overall hyperbolic kinetics of VLDL denaturation despite the presence of apoB on its surface.

In summary, we propose that sigmoidal kinetics with a lag phase observed in the heat-induced fusion of LDL (Figs. 1 and 2) is due, at least in part, to the large size and the nonexchangeable character of apoB and the absence of substantial amounts of exchangeable apolipoproteins on LDL. Sigmoidal kinetics with a lag phase is generally associated with a slightly unfavorable nucleation (51). We hypothesize that this nucleation may involve small structural changes in apoB that accumulate during the lag phase, priming LDL for fusion. These changes may alter the exposure of certain apoB epitopes that can form “sticky patches” leading to LDL pairing. The latter may involve apoB residues 405–539 (MB24 binding site) or 1022–1031 (MB11 binding site) (Fig. 5), which are located in relative proximity on LDL surface (31). We speculate that targeting conformational changes in apoB that prime LDL for fusion may provide a strategy for blocking this pathogenic reaction before it occurs.

Effects of lipoprotein concentration on fusion

Acceleration of LDL fusion upon increasing LDL concentration (Fig. 6) implies that, under conditions of our experiments, the fusion rate is limited by the collision rate of LDL. We hypothesize that, due to the nonexchangeable character of apoB and its complex energy landscape, multiple consecutive LDL collisions are required to produce structural changes on LDL surface that prime it for fusion. These changes are expected to accumulate faster upon increasing the collision rate, which helps explain the strong concentration dependence observed in LDL fusion (Fig. 6) (30). In contrast, the rate of the heat-induced HDL fusion shows no significant concentration dependence in the range explored in our work (0.15–1.0 mg/ml HDL protein), and hence, it is not limited by the collision rate in this range. In summary, the strong concentration dependence observed in LDL fusion indicates that the rate-limiting step in LDL fusion is lipoprotein collision.

Notably, LDL concentrations used in our studies (0.15–1.0 mg/ml apoB) are comparable to those found in human plasma. In fact, 0.5 mg/ml apoB corresponds to approximately 100 mg/dl LDL cholesterol, which is borderline between normal and elevated plasma levels (43), whereas LDL concentration in the arterial wall can be substantially higher. This prompts us to propose that the strong concentration dependence of LDL fusion observed in vitro (Fig. 6) is relevant to in vivo conditions. It is

well established that elevated concentrations of LDL in plasma and, particularly, in the arterial wall are highly pro-atherogenic. We hypothesize that lipoprotein fusion can contribute to this effect, as increasing LDL concentration in the near-physiologic range accelerates LDL fusion in vitro (Fig. 6), whereas reducing LDL concentration (e.g., upon administration of lipid-lowering therapies) is expected to decelerate this pathogenic reaction in vivo.


Effect of the particle size on LDL fusion: potential metabolic implications

Our results reveal that, similar to HDL (38), LDL thermal stability increases with decreasing particle diameter (Fig. 7). One possible explanation for this general trend is that smaller lipoproteins, which have higher protein-to-lipid ratio than their larger counterparts, have more extensive lipid surface coverage by the protein that hampers formation of surface packing defects. In addition, protein-protein interactions are also likely to be more extensive on smaller lipoproteins, further stabilizing these lipoproteins. Differences in the protein conformation and lipid composition may also contribute to the differences in stability of plasma LDL of different sizes. Importantly, increased structural stability of smaller denser LDL revealed in our in vitro studies implies that the enhanced pro-atherogenic properties of sdLDL are not due to their enhanced propensity to fuse but due to other factors, such as reduced affinity of sdLDL for the LDL receptor and increased affinity for the arterial proteoglycans (23–25). Furthermore, our results suggest that large LDL fuse and precipitate faster because they are less stable than sdLDL. This helps explain the mechanism underlying selective precipitation of large but not small LDL by a combination of Mg and heparin, which is used for measuring sdLDL concentrations in human plasma (25, 52). Moreover, our results are in good agreement with the report by Hurt-Camejo et al. showing that LDL subfractions that are more electronegative and have lower surface-to-core lipid ratio (i.e., larger diameter) are more prone to retention by proteoglycans and degradation by arterial macrophages (14). We speculate that lower structural stability of larger LDL contributes to the latter effect.

The effects of particle size and LDL concentration on LDL fusion observed in vitro (Figs. 6 and 7) may have potential implications for the lipid-lowering therapies. Elevated plasma levels of LDL, particularly sdLDL, are the major risk factor and a likely causative agent of atherosclerosis (23–25). Conventional lipid-lowering therapies (including statins, fibrates, niacin, and their combinations) not only improve the overall plasma levels of lipoproteins but also decrease the proportion of sdLDL and thereby increase the median size of LDL (43, 53–59). The results in Fig. 7 suggest that such an increase in size is likely to augment LDL fusion. We speculate that this potentially pro-atherogenic effect is counterbalanced by the reduction in LDL concentration upon administration of the lipid-lowering therapies, which is expected to decelerate LDL fusion (Fig. 6). Thus, we hypothesize that *i*) the lipid-lowering therapies are expected to increase LDL propensity to fuse; and *ii*) this potentially pro-atherogenic effect in vivo is probably

counterbalanced by the reduction in LDL concentration that decelerates LDL fusion. This hypothesis will be tested in future studies that will compare structural stability of LDL isolated from plasma of hyperlipidemic patients before and after treatment with lipid-lowering drugs.

Effect of pH: relevance to acidic conditions in atherosclerotic lesions

Strong pH dependence of LDL fusion reported here (Fig. 8) is consistent with recent studies of LDL hydrolyzed by sphingomyelinase or phospholipase A₂ that reported enhanced LDL aggregation, fusion, and retention by proteoglycans upon reduction in pH to mildly acidic range (Refs. 47, 60–62 and references therein). Therefore, LDL destabilization and enhanced fusion below pH 7 is a general phenomenon that is not limited to high temperatures. In fact, we observed gradual fusion of human LDL at pH 6.0, 22°C. Destabilization of LDL at mildly acidic pH may result, in part, from the reduced electrostatic repulsion between the particles upon reduction in their net charge below pH 7 (50). This destabilization likely contributes to LDL retention in the mildly acidic anaerobic environment of the atherosclerotic plaques (47, 60–62) and helps explain why LDL accumulation during atherogenesis starts in the deep areas of arterial thickening that have lowest pH (47, 63). In addition, destabilization of LDL at acidic pH is expected to promote their lysosomal degradation during normal catabolism. Although the origin of this destabilization pH effect remains unclear, large destabilization of VLDL but not HDL observed at mildly acidic pH (64) suggests that this effect is rooted, in part, in pH-induced changes in apoB. 

The authors are indebted to Dr. Shobini Jayaraman for her generous advice and help throughout this work and for the thorough reading of the manuscript prior to submission. The authors thank Cheryl England and Michael Gigliotti for help with isolation of human plasma LDL, and Dr. Yuhang Liu for help with isolation of LDL subclasses. The authors also thank Dr. Yuhang Liu and Dr. Jing Wang for help with electron microscopy. The authors are grateful to Dr. David Atkinson for his kind gift of the antibodies and for useful advice.

REFERENCES

- Segrest, J. P., M. K. Jones, H. De Loof, and N. Dashti. 2001. Structure of apolipoprotein B-100 in low density lipoproteins. *J. Lipid Res.* **42**: 1346–1367.
- Goldstein, J. L., and M. S. Brown. 1976. The LDL pathway in human fibroblasts: a receptor-mediated mechanism for the regulation of cholesterol metabolism. *Curr. Top. Cell. Regul.* **11**: 147–181.
- Castelli, W. P., K. Anderson, P. W. Wilson, and D. Levy. 1992. Lipids and risk of coronary heart disease. The Framingham Study. *Ann. Epidemiol.* **2**: 23–28.
- Williams, K. J., and I. Tabas. 1995. The response-to-retention hypothesis of early atherogenesis. *Arterioscler. Thromb. Vasc. Biol.* **15**: 551–561.
- Camejo, G., E. Hurt-Camejo, O. Wiklund, and G. Bondjers. 1998. Association of apo B lipoproteins with arterial proteoglycans: pathological significance and molecular basis. *Atherosclerosis.* **139**: 205–222.
- Skälén, K., M. Gustafsson, E. K. Rydberg, L. M. Hultén, O. Wiklund, T. L. Innerarity, and J. Borén. 2002. Subendothelial retention of

- atherogenic lipoproteins in early atherosclerosis. *Nature.* **417**: 750–754.
- Tabas, I., K. J. Williams, and J. Borén. 2007. Subendothelial lipoprotein retention as the initiating process in atherosclerosis: update and therapeutic implications. *Circulation.* **116**: 1832–1844.
- Fogelstrand, P., and J. Borén. 2012. Retention of atherogenic lipoproteins in the artery wall and its role in atherogenesis. *Nutr. Metab. Cardiovasc. Dis.* **22**: 1–7.
- Oörni, K., M. O. Pentikäinen, M. Ala-Korpela, and P. T. Kovanen. 2000. Aggregation, fusion, and vesicle formation of modified low density lipoprotein particles: molecular mechanisms and effects on matrix interactions. *J. Lipid Res.* **41**: 1703–1714.
- Oörni, K., and P. T. Kovanen. 2009. Lipoprotein modification by secretory phospholipase A(2) enzymes contributes to the initiation and progression of atherosclerosis. *Curr. Opin. Lipidol.* **20**: 421–427.
- Plihtari, R., E. Hurt-Camejo, K. Oörni, and P. T. Kovanen. 2010. Proteolysis sensitizes LDL particles to phospholipolysis by secretory phospholipase A2 group V and secretory sphingomyelinase. *J. Lipid Res.* **51**: 1801–1809.
- Hakala, J. K., K. Oorni, M. O. Pentikainen, E. Hurt-Camejo, and P. T. Kovanen. 2001. Lipolysis of LDL by human secretory phospholipase A(2) induces particle fusion and enhances the retention of LDL to human aortic proteoglycans. *Arterioscler. Thromb. Vasc. Biol.* **21**: 1053–1058.
- Schissel, S. L., X. Jiang, J. Tweedie-Hardman, T. Jeong, E. H. Camejo, J. Najib, J. H. Rapp, K. J. Williams, and I. Tabas. 1998. Secretory sphingomyelinase, a product of the acid sphingomyelinase gene, can hydrolyze atherogenic lipoproteins at neutral pH. *J. Biol. Chem.* **273**: 2738–2746.
- Hurt-Camejo, E., G. Camejo, B. Rosengren, F. López, O. Wiklund, and G. Bondjers. 1990. Differential uptake of proteoglycan-selected subfractions of low density lipoprotein by human macrophages. *J. Lipid Res.* **31**: 1387–1398.
- Mateu, L., E. M. Avila, V. León, and N. Liscano. 1984. The structural stability of low density lipoprotein: a kinetic X-ray scattering study of its interaction with arterial wall proteoglycans. *Biochim. Biophys. Acta.* **795**: 525–534.
- Khoo, J. C., E. Miller, P. McLoughlin, and D. Steinberg. 1988. Enhanced macrophage uptake of low density lipoprotein after self-aggregation. *Arteriosclerosis.* **8**: 348–358.
- Bancell, C., S. Villegas, F. J. Blanco, S. Benitez, I. Gallego, L. Beloki, M. Perez-Cuellar, J. Ordonez-Llanos, and J. L. Sanchez-Quesada. 2010. Aggregated electronegative low-density lipoprotein in human plasma shows high tendency to phospholipolysis and particle fusion. *J. Biol. Chem.* **285**: 32425–32435.
- Johs, A., M. Hammel, I. Waldner, R. P. May, P. Laggner, and R. Prassl. 2006. Modular structure of solubilized human apolipoprotein B-100. Low resolution model revealed by small angle neutron scattering. *J. Biol. Chem.* **281**: 19732–19739.
- Prassl, R., and P. Laggner. 2009. Molecular structure of low density lipoprotein: current status and future challenges. *Eur. Biophys. J.* **38**: 145–158.
- Liu, Y., and D. Atkinson. 2011. Immuno-electron cryo-microscopy imaging reveals a looped topology of apoB at the surface of human LDL. *J. Lipid Res.* **52**: 1111–1116.
- Kumar, V., S. J. Butcher, K. Öörni, P. Engelhardt, J. Heikkinen, K. Kaski, M. Ala-Korpela, and P. T. Kovanen. 2011. Three-dimensional cryoEM reconstruction of native LDL particles to 16Å resolution at physiological body temperature. *PLoS ONE.* **6**: e18841.
- McNamara, J. R., D. M. Small, Z. Li, and E. J. Schaefer. 1996. Differences in LDL subspecies involve alterations in lipid composition and conformational changes in apolipoprotein B. *J. Lipid Res.* **37**: 1924–1935.
- Kwiterovich, P. O., Jr. 2002. Clinical relevance of the biochemical, metabolic, and genetic factors that influence low-density lipoprotein heterogeneity. *Am. J. Cardiol.* **90(8A)**: 30i–47i.
- Krauss, R. M. 2010. Lipoprotein subfractions and cardiovascular disease risk. *Curr. Opin. Lipidol.* **21**: 305–311.
- Ai, M., S. Ootokozawa, B. F. Asztalos, Y. Ito, K. Nakajima, C. C. White, L. A. Cupples, P. W. Wilson, and E. J. Schaefer. 2010. Small dense LDL cholesterol and coronary heart disease: results from the Framingham Offspring Study. *Clin. Chem.* **56**: 967–976.
- Sánchez-Quesada, J. L., S. Benítez, and J. Ordóñez-Llanos. 2004. Electronegative low-density lipoprotein. *Curr. Opin. Lipidol.* **15**: 329–335.

27. Gaubatz, J. W., B. K. Gillard, J. B. Massey, R. C. Hoogeveen, M. Huang, E. E. Lloyd, J. L. Raya, C. Y. Yang, and H. J. Pownall. 2007. Dynamics of dense electronegative low density lipoproteins and their preferential association with lipoprotein phospholipase A(2). *J. Lipid Res.* **48**: 348–357.
28. Bancells, C., S. Benítez, J. Ordóñez-Llanos, K. Öörni, P. T. Kovanen, R. W. Milne, and J. L. Sánchez-Quesada. 2011. Immunochemical analysis of the electronegative LDL subfraction shows that abnormal N-terminal apolipoprotein B conformation is involved in increased binding to proteoglycans. *J. Biol. Chem.* **286**: 1125–1133.
29. Khoo, J. C., E. Miller, P. McLoughlin, and D. Steinberg. 1990. Prevention of low density lipoprotein aggregation by high density lipoprotein or apolipoprotein A-I. *J. Lipid Res.* **31**: 645–652.
30. Jayaraman, S., D. L. Gantz, and O. Gursky. 2005. Structural basis for thermal stability of human low-density lipoprotein. *Biochemistry.* **44**: 3965–3971.
31. De Spirito, M., R. Brunelli, G. Mei, F. R. Bertani, G. Ciasca, G. Greco, M. Papi, G. Arcovito, F. Ursini, and T. Parasassi. 2006. Low density lipoprotein aged in plasma forms clusters resembling sub-endothelial droplets: aggregation via surface sites. *Biophys. J.* **90**: 4239–4247.
32. Jayaraman, S., D. L. Gantz, and O. Gursky. 2011. Effects of phospholipase A2 and its products on structural stability of human low-density lipoprotein: Relevance to formation of LDL-derived lipid droplets. *J. Lipid Res.* **52**: 549–557.
33. Gursky, O., Ranjana, and D. L. Gantz. 2002. Complex of human apolipoprotein C-1 with phospholipid: thermodynamic or kinetic stability? *Biochemistry.* **41**: 7373–7384.
34. Mehta, R., D. L. Gantz, and O. Gursky. 2003. Human plasma high-density lipoproteins are stabilized by kinetic factors. *J. Mol. Biol.* **328**: 183–192.
35. Jayaraman, S., D. L. Gantz, and O. Gursky. 2006. Effects of salt on thermal stability of human plasma high-density lipoproteins. *Biochemistry.* **45**: 4620–4628.
36. Guha, M., C. O. England, H. Herscovitz, and O. Gursky. 2007. Thermal transitions in human very low-density lipoprotein: fusion, rupture and dissociation of HDL-like particles. *Biochemistry.* **46**: 6043–6049.
37. Guyton, J. R., and K. F. Klemp. 1994. Development of the atherosclerotic core region. Chemical and ultrastructural analysis of microdissected atherosclerotic lesions from human aorta. *Arterioscler. Thromb.* **14**: 1305–1314.
38. Gao, X., S. Yuan, S. Jayaraman, and O. Gursky. 2009. Differential stability of high-density lipoprotein subclasses: effects of particle size and protein composition. *J. Mol. Biol.* **387**: 628–638.
39. Schumaker, V. N., and D. L. Puppione. 1986. Sequential flotation ultracentrifugation. *Methods Enzymol.* **128**: 155–170.
40. Markwell, M. A., S. M. Haas, L. L. Bieber, and N. E. Tolbert. 1978. A modification of the Lowry procedure to simplify protein determination in membrane and lipoprotein samples. *Anal. Biochem.* **87**: 206–210.
41. Guha, M., D. L. Gantz, and O. Gursky. 2008. Effect of fatty acyl chain length, unsaturation and pH on the stability of discoidal high-density lipoproteins. *J. Lipid Res.* **49**: 1752–1761.
42. Wallace, B. A., and C. L. Teeters. 1987. Differential absorption flattening optical effects are significant in the circular dichroism spectra of large membrane fragments. *Biochemistry.* **26**: 65–70.
43. Ballantyne, C. M., J. S. Raichlen, and V. A. Cain. 2008. Statin therapy alters the relationship between apolipoprotein B and low-density lipoprotein cholesterol and non-high-density lipoprotein cholesterol targets in high-risk patients: the MERCURY II (Measuring Effective Reductions in Cholesterol Using Rosuvastatin) trial. *J. Am. Coll. Cardiol.* **52**: 626–632.
44. Margolis, S. 1967. Separation and size determination of human serum lipoproteins by agarose gel filtration. *J. Lipid Res.* **8**: 501–507.
45. Jayaraman, S., D. L. Gantz, and O. Gursky. 2005. Kinetic stabilization and fusion of discoidal lipoproteins containing human apoA-2 and DMPC: comparison with apoA-1 and apoC-1. *Biophys. J.* **88**: 2907–2918.
46. Gao, X., S. Jayaraman, M. Guha, J. Wally, M. Lu, D. Atkinson, and O. Gursky. 2012. Application of circular dichroism to lipoproteins: structure, stability and remodeling of good and bad cholesterol. In *Circular Dichroism: Theory and Spectroscopy*. D. S. Rogers, editor. Nova Publishers, Hauppauge, NY. 175–215.
47. Sneek, M., S. D. Nguyen, T. Pihlajamaa, G. Yohannes, M.-L. Riekkola, R. W. Milne, P. T. Kovanen, and K. Oorni. Conformational changes of apoB-100 in sphingomyelinase-modified LDL mediate formation of large aggregates at acidic pH. *J. Lipid Res.* Epub ahead of print. June 20, 2012; doi:10.1194/jlr.M023218.
48. Liu, H., D. G. Scraba, and R. O. Ryan. 1993. Prevention of phospholipase-C induced aggregation of low density lipoprotein by amphipathic apolipoproteins. *FEBS Lett.* **316**: 27–33.
49. Pentikäinen, M. O., M. T. Hyvönen, K. Öörni, T. Hevonoja, A. Korhonen, E. M. Lehtonen-Smeds, M. Ala-Korpela, and P. T. Kovanen. 2001. Altered phospholipid-apoB-100 interactions and generation of extra membrane material in proteolysis-induced fusion of LDL particles. *J. Lipid Res.* **42**: 916–922.
50. Melnik, B. C., and S. F. Melnik. 1988. Analytical isoelectric focusing of apolipoprotein B of human plasma low-density lipoproteins in the presence of a nonionic and a zwitterionic detergent. *Anal. Biochem.* **171**: 320–329.
51. Kodaka, M. 2004. Requirements for generating sigmoidal time-course aggregation in nucleation-dependent polymerization model. *Biophys. Chem.* **107**: 243–253.
52. Hirano, T., Y. Ito, H. Saegusa, and G. Yoshino. 2003. A novel and simple method for quantification of small, dense LDL. *J. Lipid Res.* **44**: 2193–2201.
53. Morgan, J. M., D. M. Capuzzi, R. I. Baksh, C. Intenzo, C. M. Carey, D. Reese, and K. Walker. 2003. Effects of extended-release niacin on lipoprotein subclass distribution. *Am. J. Cardiol.* **91**: 1432–1436.
54. Baldassarre, S., O. Scruel, R. J. Deckelbaum, I. E. Dupont, J. Ducobu, and Y. A. Carpentier. 2005. Beneficial effects of atorvastatin on sd LDL and LDL phenotype B in statin-naïve patients and patients previously treated with simvastatin or pravastatin. *Int. J. Cardiol.* **104**: 338–345.
55. Backes, J. M., and C. A. Gibson. 2005. Effect of lipid-lowering drug therapy on small-dense low-density lipoprotein. *Ann. Pharmacother.* **39**: 523–526.
56. Tribble, D. L., M. Farnier, G. Macdonell, I. Perevozskaya, M. J. Davies, B. Gumbiner, and T. A. Musliner. 2008. Effects of fenofibrate and ezetimibe, both as monotherapy and in coadministration, on cholesterol mass within lipoprotein subfractions and low-density lipoprotein peak particle size in patients with mixed hyperlipidemia. *Metabolism.* **57**: 796–801.
57. Florentin, M., A. D. Tselepis, M. S. Elisaf, C. V. Rizos, D. P. Mikhailidis, and E. N. Liberopoulos. 2010. Effect of non-statin lipid lowering and anti-obesity drugs on LDL subfractions in patients with mixed dyslipidaemia. *Curr. Vasc. Pharmacol.* **8**: 820–830.
58. McCullough, P. A., A. B. Ahmed, M. T. Zughaib, E. D. Glanz, and M. J. Di Loreto. 2011. Treatment of hypertriglyceridemia with fibric acid derivatives: impact on lipid subfractions and translation into a reduction in cardiovascular events. *Rev. Cardiovasc. Med.* **12**: 173–185.
59. Sampson, U. K., S. Fazio, and M. F. Linton. 2012. Residual cardiovascular risk despite optimal LDL cholesterol reduction with statins: the evidence, etiology, and therapeutic challenges. *Curr. Atheroscler. Rep.* **14**: 1–10.
60. Öörni, K., and P. T. Kovanen. 2006. Enhanced extracellular lipid accumulation in acidic environments. *Curr. Opin. Lipidol.* **17**: 534–540.
61. Lähdesmäki, K., R. Plihtari, P. Soiminen, E. Hurt-Camejo, M. Ala-Korpela, K. Öörni, and P. T. Kovanen. 2009. Phospholipase A(2)-modified LDL particles retain the generated hydrolytic products and are more atherogenic at acidic pH. *Atherosclerosis.* **207**: 352–359.
62. Lähdesmäki, K., K. Öörni, M. Alanne-Kinnunen, M. Jauhiainen, E. Hurt-Camejo, and P. T. Kovanen. 2012. Acidity and lipolysis by group V secreted phospholipase A(2) strongly increase the binding of apoB-100-containing lipoproteins to human aortic proteoglycans. *Biochim. Biophys. Acta.* **1821**: 257–267.
63. Nakashima, Y., T. N. Wight, and K. Sueishi. 2008. Early atherosclerosis in humans: role of diffuse intimal thickening and extracellular matrix proteoglycans. *Cardiovasc. Res.* **79**: 14–23.
64. Guha, M., and O. Gursky. 2011. Human plasma very low-density lipoproteins are stabilized by electrostatic interactions and destabilized by acidic pH. *J. Lipids.* **2011**: 493720.